



Universiteit
Leiden
The Netherlands

Spin-transition frameworks based on bistetrazole and triazine ligands

Quesada Vilar, Manuel

Citation

Quesada Vilar, M. (2007, March 29). *Spin-transition frameworks based on bistetrazole and triazine ligands*. Retrieved from <https://hdl.handle.net/1887/11463>

Version: Corrected Publisher's Version

License: [Licence agreement concerning inclusion of doctoral thesis in the Institutional Repository of the University of Leiden](#)

Downloaded from: <https://hdl.handle.net/1887/11463>

Note: To cite this publication please use the final published version (if applicable).

A Molecular Nanoporous Material Showing Tuneable Spin-Crossover near Room Temperature

Abstract

From a molecular approach, the search for multifunctional materials is one of the main targets of contemporary material science. Among these, the inclusion of a spin-crossover functionality is especially appealing; as such materials may act as room temperature switches by responding to different types of external perturbations, e.g. temperature, pressure, light or a magnetic field. This chapter deals with a 1D open-framework hybrid organic-inorganic compound, i.e. $[\text{Fe}_3(\text{dpyatriz})_2(\text{BF}_4)_2(\text{CH}_3\text{CH}_2\text{CN})_4](\text{BF}_4)_4 \cdot 4(\text{CH}_3\text{CH}_2\text{CN})$, exhibiting a thermal spin-crossover centred at room temperature. In addition, this material shows a structural, magnetic and chromatic reversible response to a sorption/desorption process. The accessibility of the Fe^{II} spin-crossover centres through the open channels of the porous materials permits the tuning of the spin-transition properties of the material by choosing the appropriate solvent, thus revealing the first example of a bi-functional material, where the host-guest properties – via coordinative bonding – directly influence the physical properties of the metallic sites.

Part of this chapter has appeared in literature: Quesada, M; de la Peña-O'Shea, V. A., Aromí, G; Geremia, S; Massera, C; Roubeau, O; Gamez, P; Reedijk, J. accepted in *Advanced Materials*.

8.1 Introduction.

One of the great challenges underlying the search of molecule-based functional materials is to produce systems exhibiting properties of technological interest that can be tuned and exploited at room temperature. Some landmark achievements in this respect are the discovery of a molecule-based magnet displaying ordering above 300 °C,¹ or the preparation of molecular materials undergoing spin-crossover phenomena near room temperature (Chapter 1, section 1.1).² Spin-crossover materials are based on the capacity of certain transition metal ions to interconvert between two stable electronic states with concomitant switching of their colour, magnetic properties and/or molecular structural parameters.^{3, 4} The transition is triggered by external stimuli, such as electromagnetic radiation, magnetic fields or pressure/temperature variations. Within crystalline phases, the response to the spin-crossover may be transmitted in a cooperative manner throughout the material, leading to a sharp transition and sometimes to a hysteretic behaviour.⁵ In such a case, the system becomes bi-stable and can therefore be contemplated as an externally addressable molecular switch. Current efforts are aimed at integrating spin-crossover centres into metal organic frameworks (MOFs) in order to combine the properties derived from the spin transition with other properties, such as chirality, conductivity or those derived from nanoporosity. The molecular approach used in preparing hybrid materials has been mostly exploited to obtain networks exhibiting a wide range of pore sizes and shapes,⁶⁻⁸ with the added potential of offering various other functions, in particular thanks to the inclusion of transition metals.⁹⁻¹¹ This may lead to systems where the multifunctionality is manifested by the coexistence of more than one property, such as ferromagnetism and metallic conductivity,¹² with no mutual interdependence. The presence of different functions within a material, however, can occur in such a way that they influence each other in a synergetic manner, producing effects that would not be observed if these properties were not coupled. Remarkable examples are, for instance, the observation of a switchable dielectric constant in a material controlled by the spin-state of its spin-crossover centres,¹³ or the ability to modify the spin-crossover properties of a nanoporous framework by changing the nature of its guest molecules.¹⁴

The design and synthesis of sophisticated multidentate N-heterocyclic ligands such as dpyatriz (dpyatriz = 2,4,6-tris-(di(pyridin-2-yl)amino)-1,3,5-triazine; Figure 8.1 a)¹⁵ and the study of their ability to combine with paramagnetic ions in the construction of zero-dimensional or polymeric metal-organic arrays with interesting magnetic properties have attracted much interest. For example, metal-organic open frameworks with unprecedented structures that include open-shell metals have been fully characterised.^{16, 17} In addition, discrete dinuclear complexes of Fe^{II} with dpyatriz have been obtained, that display ferromagnetic exchange (extremely rare), or spin-crossover properties that can be easily modulated by changing the solvent used, that acts as a terminal ligand (Figure 8.1 b, see chapter 6).¹⁸ The use of such dimeric units as building blocks in solvothermal reactions involving Fe^{II} has now taken this chemistry one step further and has provided access to a new metal-organic nanoporous material exhibiting room-temperature spin-crossover behaviour. The structure of this material can be modified reversibly through exposure to various solvents, the transformation leading to significant changes in the spin-transition properties. The porosity of the material enables the solvent exchange and is thus responsible for the

observation of a room-temperature spin-crossover material whose properties can be modulated, *via* its nanostructure, by the control over the external composition of the atmosphere. This chapter deals with the solvent dependency of the spin-transition properties of the 1D polymer $[\text{Fe}_3(\text{dpyatriz})_2(\text{BF}_4)_2(\text{CH}_3\text{CH}_2\text{CN})_4](\text{BF}_4)_4 \cdot 4(\text{CH}_3\text{CH}_2\text{CN})$ (**14**). X-ray powder diffraction experiments at variable temperature and different solvent atmospheres are presented. The substitution with non-volatile molecules that leads to other spin-transition behaviours is also studied.

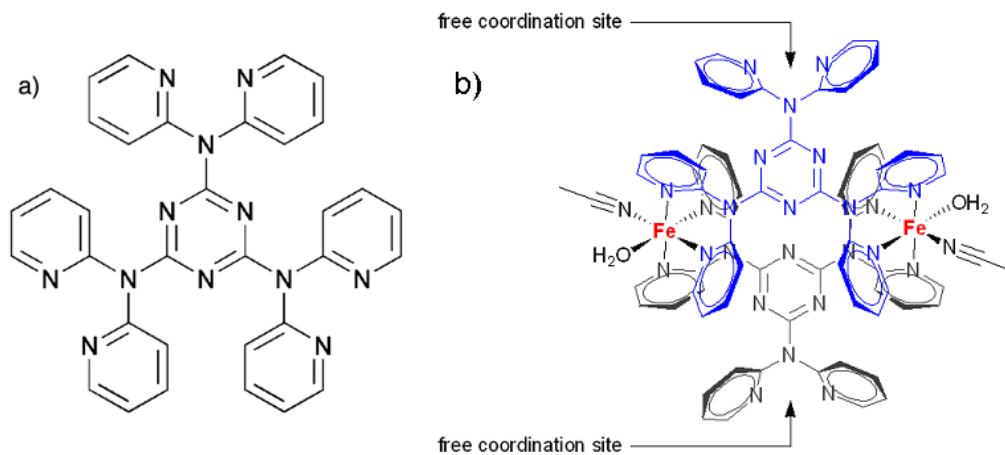


Figure 8.1. a) Dpyatriz = 2,4,6-tris-(di(pyridine-2-yl)amino)-1,3,5-triazine. b) Dinuclear complex presented in chapter 6 showing free coordination sites.

Table 8.1. Crystal data and structure refinement for **14**.

Formula	$\text{C}_{95}\text{H}_{88}\text{Fe}_3\text{N}_{32}\text{B}_6\text{F}_{24}$ $\text{Fe}_3(\text{C}_{66}\text{H}_{48}\text{N}_{24})(\text{BF}_4)_6(\text{C}_3\text{H}_5\text{N})_8$
Fw	1153.1
T, K	100 (2)
λ , Å	1.000
Cryst. system, space group	Triclinic, <i>P</i> -1
<i>a</i> , <i>b</i> , <i>c</i> , Å	13.797(1) 14.783(1) 14.731(1)
α , β , γ , deg	81.46(1) 74.72(1) 65.18(1)
<i>V</i> , Å ³	2628.2(4)
<i>Z</i> , <i>D</i> _{calc} g/cm ³	1, 1.46
μ , mm ⁻¹	1.228
<i>F</i> (000)	1175.7
$\lambda/2\text{sen}\theta_{\text{max}}$, Å	0.95
Reflns measured	21115
Reflns unique	5535
Reflns <i>I</i> >2.0 σ (<i>I</i>)	5227
Rmerge	0.017 (0.040, in shell 0.98 Å-0.95 Å)
Extinction coefficient	0.034
Params	783
restraints	397
G.o.f.	1.053
<i>R</i> [<i>I</i> >2 σ (<i>I</i>)]	<i>R</i> 1 = 0.083, w <i>R</i> 2 = 0.233
<i>R</i> (all data)	<i>R</i> 1 = 0.086, w <i>R</i> 2 = 0.236
Residuals max min, e/Å ³	0.621, -0.751

Table 8.2. Selected interatomic distances [Å] and angles [°] for $[\text{Fe}_3(\text{dpyatriz})_2(\text{BF}_4)_2(\text{CH}_3\text{CH}_2\text{CN})_4](\text{BF}_4)_4 \cdot 4(\text{CH}_3\text{CH}_2\text{CN})$

Compound $[\text{Fe}_3(\text{dpyatriz})_2(\text{BF}_4)_2(\text{CH}_3\text{CH}_2\text{CN})_4](\text{BF}_4)_4 \cdot 4(\text{CH}_3\text{CH}_2\text{CN})$			
Fe1-F1a	2.2629(66)	N10-Fe1-F1a b	91.07(20)
Fe1-N9	2.1682(49)	N10-Fe1-N9 b	95.26(20)
Fe1-N10	2.1814(54)	N7-Fe2-N8	87.93(23)
Fe2-N7	2.0370(60)	N7-Fe2-N13	87.78(25)
Fe2-N8	2.0448(56)	N7-Fe2-N14	177.33(21)
Fe2-N13	1.9797(58)	N7-Fe2-11 a	92.66(23)
Fe2-N14	2.0011(71)	N7-Fe2-12 a	95.74(18)
Fe2-N11a	2.0433(55)	N8-Fe2-N13	88.46(24)
Fe2-N12a	2.0309(44)	N8-Fe2-N14	91.78(24)
F1a-Fe1-N9	89.10(20)	N8-Fe2-11 a	179.37(23)
F1a-Fe1-N10	88.93(20)	N8-Fe2-12 a	92.72(17)
F1a-Fe1-F1a b	180.00	N13-Fe2-N14	89.56(27)
F1a-Fe1-N9 b	90.90(20)	N13-Fe2-11 a	91.36(24)
F1a-Fe1-N10 b	91.07(20)	N13-Fe2-12 a	176.31(25)
N9-Fe1-N10	84.74(20)	N14-Fe2-N11 a	87.62(24)
N9-Fe1-F1a b	90.90(20)	N14-Fe2- N12 a	86.92(21)
N9-Fe1-N9 b	180.00	N11 a-Fe2-N12 a	87.42(17)
N9-Fe1-N10 b	95.26(20)	Fe1...Fe1	15.416

8.2 $[\text{Fe}_3(\text{dpyatriz})_2(\text{BF}_4)_2(\text{CH}_3\text{CH}_2\text{CN})_4](\text{BF}_4)_4 \cdot 4(\text{CH}_3\text{CH}_2\text{CN})$: synthesis and description.

Reactions of dpyatriz with Fe^{II} salts at ambient conditions (room temperature and atmospheric pressure) result in dinuclear compounds (irrespective of the Fe/ligand ratio used, from 1:1 to 3:1), comprising two iron centres bridged by two dpyatriz ligands (Figure 8.1), some of them exhibiting spin–crossover properties.¹⁸ These complexes feature two free binding sites for metals, and can therefore be used as building blocks in the preparation of spin-transition extended structures.

The application of solvothermal conditions to one of the aforementioned systems in propionitrile (with an increased Fe/ligand ratio of 3:2), leads to the formation of a new molecular material, consisting of 1D polymeric chains, **14**, as revealed by single crystal X-ray studies (Figure 8.1 a, Table 8.1). These chains originate from the previously identified dinuclear $[\text{Fe}_2]$ building blocks, assembled *via* their free coordination pockets, by additional Fe^{II} centres (Figure 8.2 b). At high temperatures (95 °C) the compound crystallises as white parallelepipeds, which on cooling to room temperature turn purple.^a

^a See chapter 2 for details on the experimental procedures and recipes for all compounds presented in this chapter.

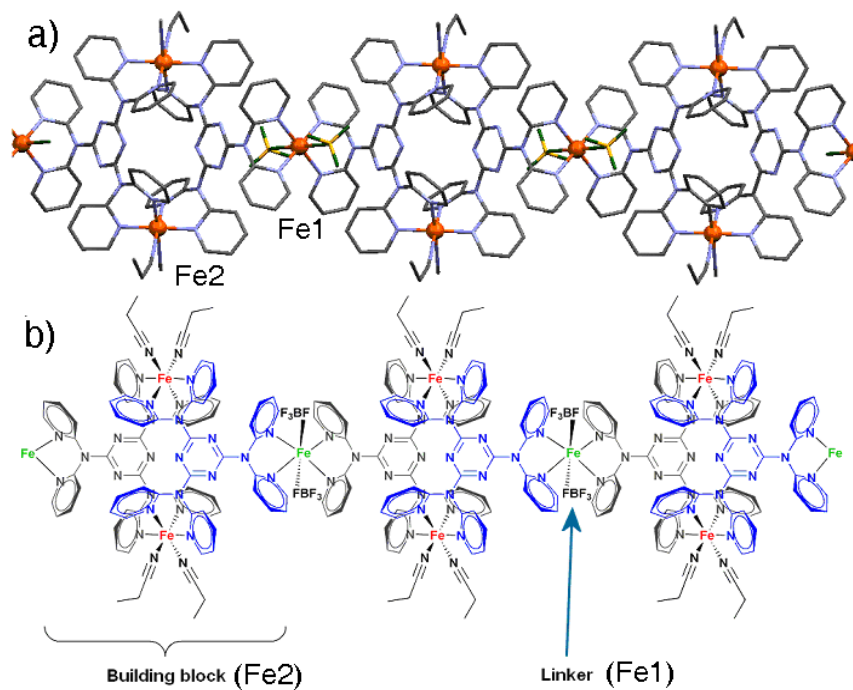


Figure 8.2. Left, view of the X-ray crystal structure of the 1D polymeric chain of **14** (a), and schematic representation of this view emphasizing the dimers (formed by Fe2 centres) bridged by individual iron(II) ions (Fe1) (b).

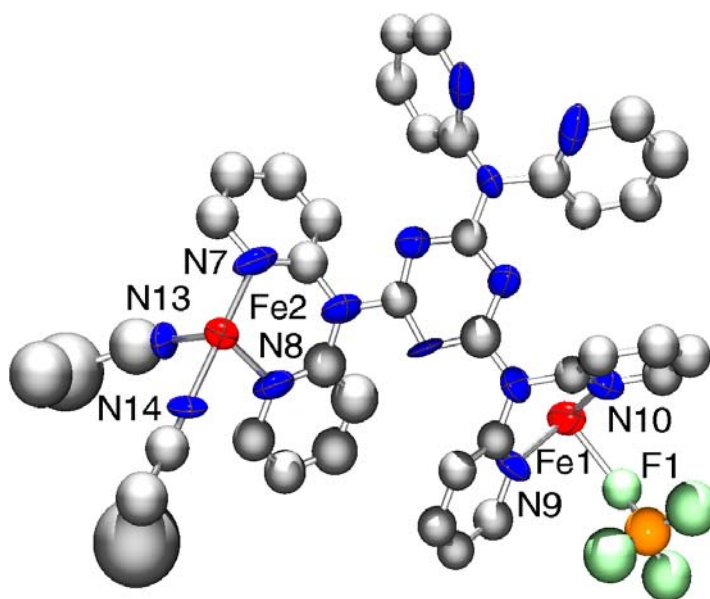


Figure 8.3 ORTEP (Oak Ridge thermal ellipsoid plot) at 50% probability level of the asymmetric unit of **14**. Fe1 has a tetrafluoroborate anion axially coordinated, while Fe2 has propionitrile molecules completing the coordination sphere.

$[\text{Fe}_3(\text{dpyatriz})_2(\text{BF}_4)_2(\text{CH}_3\text{CH}_2\text{CN})_4](\text{BF}_4)_4 \cdot 4(\text{CH}_3\text{CH}_2\text{CN})$ contains two chemically distinct and crystallographically independent types of Fe^{II} ions (Figure 8.3); (i) two ions ($\text{Fe}2$) corresponding to the original building block, and (ii) one metal centre ($\text{Fe}1$) connecting dimers pairwise to generate infinite chains (Figure 8.2). $\text{Fe}2$ has a distorted octahedral environment in which four positions are occupied by the aromatic N-donors of two dipyridylamino moieties from different dpyatriz ligands while the remaining positions are occupied by two propionitrile solvent molecules disposed in *cis* configuration. All Fe–N distances are in the range expected for a low-spin (LS) Fe^{II} centre³ (see Table 8.2). The coordination geometry of $\text{Fe}1$ is also distorted octahedral, with two chelating dipyridylamino moieties coordinated in the equatorial plane and two tetrafluoroborate anions at the axial positions. The Fe–N distances within this chromophore are in the normal range for high-spin (HS) Fe^{II} centres³ (see Table 8.2). The crystal packing of the infinite chains of **14** leads to a nanostructured material exhibiting channel-like cavities (with a cross-section of about $6 \times 4 \text{ \AA}$) that host lattice-solvent molecules, and non-coordinated tetrafluoroborate anions. These channels also accommodate the ethyl groups of the coordinated propionitrile molecules (Figure 8.4). Specific surface area measurements for **14** have been done using a standard procedure for a ThermoQuest Analyzer. **14** is purged under nitrogen during 2 hours at a temperature of $150 \text{ }^\circ\text{C}$. The sample (now light yellow, since the propionitrile molecules have desorbed at this temperature, under the nitrogen flux) is cooled to 77 K under a flow of N_2 gas. The surface area for **14** after desorption is $0.55 \text{ m}^2 \text{ g}^{-1}$. This is a rather small but not negligible value, which characterises the presence of channels that give accessibility to the labile ligands of $\text{Fe}2$ making this ion susceptible to chemical functionalisation (i.e. *via* solvent or ligand exchange, see below).¹⁹

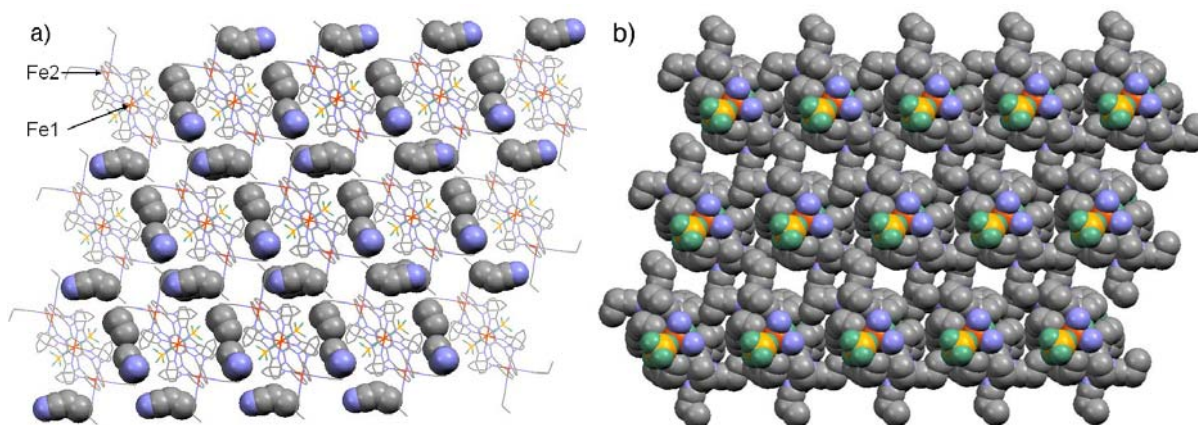


Figure 8.4. a) Representation of the crystal lattice of **14**, showing the space-filling occupation by the solvent molecules (propionitrile) of the cavities formed among the polymeric chains. Hydrogen atoms and non-coordinated counterions have been omitted for clarity, as well as positional disorder of certain molecules. b) View of the $6 \times 4 \text{ \AA}$ cross-section cavities present in the crystal packing of **14** after omission of the solvent molecules. Non-coordinated BF_4^- ions and hydrogen atoms have been omitted for clarity.

8.3 Reactivity of $[\text{Fe}_3(\text{dpyatriz})_2(\text{BF}_4)_2(\text{CH}_3\text{CH}_2\text{CN})_4](\text{BF}_4)_4 \cdot 4(\text{CH}_3\text{CH}_2\text{CN})$

8.3.1 Reaction with water.

When single crystals of **14** are removed from their mother liquor, they rapidly lose their purple colour and subsequently their crystallinity, transforming into a yellow insoluble powder. Thorough analysis of the resulting material (**15**) by IR, elemental analysis and TGA (see Figure 8.5) reveals that all the propionitrile molecules present in the initial compound have been replaced by water molecules. As observed in Figure 8.5, there are two peaks in the DTG diagram that can be assigned to the loss of both the lattice water molecules and the coordinated water molecules. The high temperatures at which the lattice water molecules are desorbed suggest strong hydrogen bonding interactions (see below). Coordinated water molecules are abstracted in the range of temperatures observed for other 1D polymeric spin-transition materials.²⁰ In the dpyatriz-based systems, a related exchange process in the solid state has been previously observed¹⁸ and presented in chapter 6, which led to important changes of the magnetic properties of the material.

Attempts to follow any possible structural changes accompanying the host–guest transition of **14** have faced difficulties caused by the rate of the process, which resulted in rapid loss of crystallinity. This shortcoming has been overcome by following the exchange through X-ray powder diffraction (XRPD) under a saturated atmosphere of propionitrile (also containing atmospheric water). As seen in Figure 8.6, the desorption of the propionitrile takes place during a gradual increase of the temperature. This has permitted to unveil that indeed a distinct structural phase is involved in the transformation that has proven to be reversible. Thus, as **15** is immersed again in propionitrile, the compound is found to recover its original purple colour and all the other features of the XRPD pattern that characterise the structure of the initial **14** material.

These experiments confirm that the host material exchanges all its propionitrile guest-molecules by atmospheric water molecules from the atmosphere. The examination of the XRPD diffractograms has revealed that this exchange causes a shortening of the distances separating the polymer chains within the material with the subsequent reduction of the size of the nanopores. This diminution of the inter–chain distance is evident from the fact that the two main peaks of the diffraction patterns, which arise from the [010] and [111] crystallographic planes and correspond to the interpolymeric distances (see Figure 8.7), shift towards higher 2θ values upon replacement of propionitrile by water. The likely reasons for this contraction are the smaller volume of the incoming water molecules, and the ability of these molecules to establish hydrogen bonding interactions within the coordination network. In fact, the interplanar distances of compounds involving water molecules show powder diffraction peaks between 8 and 9°,²¹ as observed for **15**. Similar changes in structure upon exchange of lattice solvents with preservation of the crystallinity have been recently reported for other 1D coordination polymers.²² In the case of the **14** to **15** transformation, it has to be mentioned that if the process is performed very fast, the system loses part, or all, of its crystallinity.

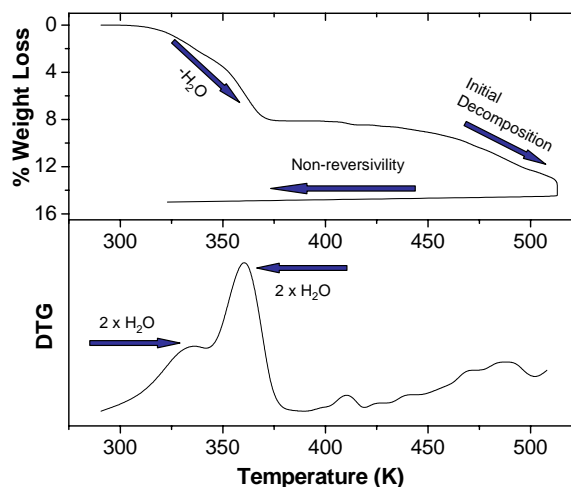


Figure 8.5. Plot of the weight-loss vs. temperature of **15**. The first derivative of the process (DTG) is also plotted.

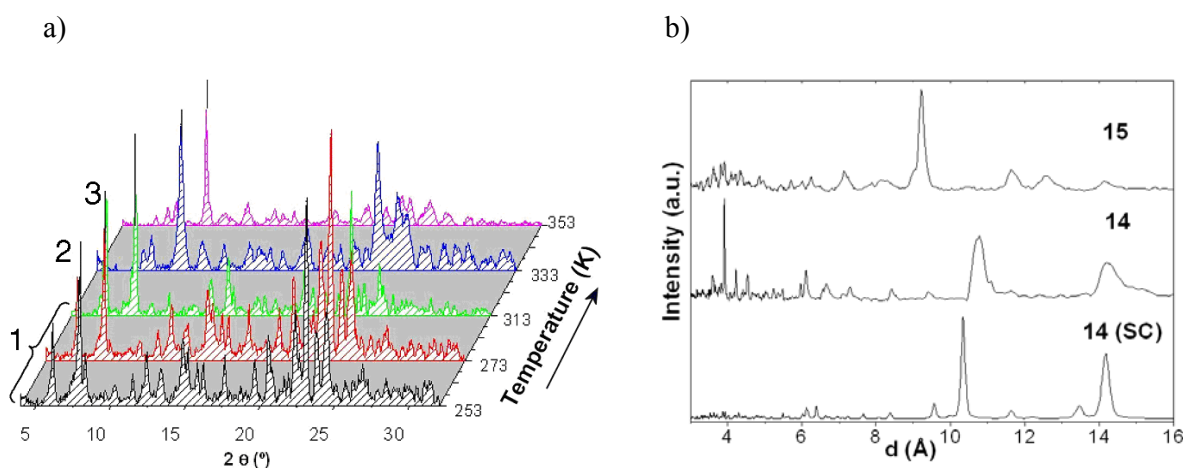
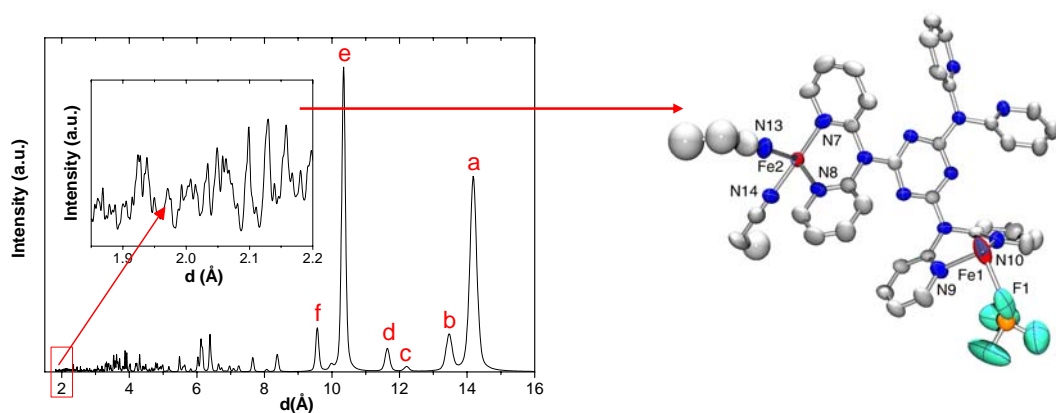
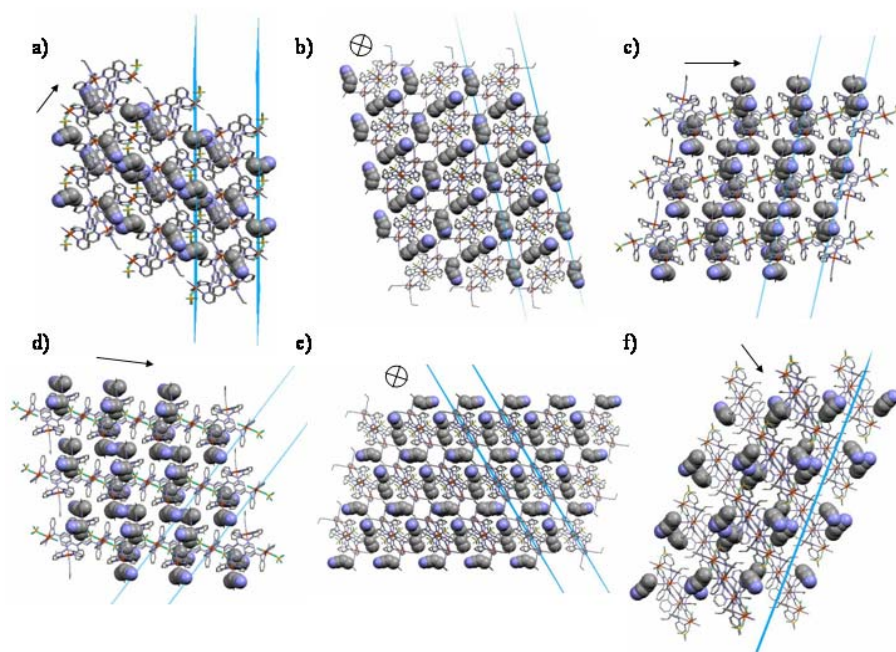


Figure 8.6. a) X-ray powder diffractograms showing the transformation of **14** (253 K), into **15** (353 K) in the presence of atmospheric water and saturated propionitrile vapour, upon increasing the temperature. 1) XRPD patterns corresponding to **14**; 2) XRPD pattern corresponding to a mixture [**14** + **15**], suggesting that, at no point, the transformation goes through an amorphous phase (since the two phases coexist at 333 K); 3) XRPD pattern corresponding to **15**. b) Comparison of the XRPD patterns of **14** and **15** with the XRPD pattern of **14** calculated from the CIF of the single-crystal X-ray structure. The slight differences observed in the distances between the calculated and the measured spectra of **14** may be due to the distinct temperatures of measurements (100 K and 253 K, respectively). These different experimental conditions can also explain the broadening of the peaks observed in the measured diffractogram. The temperatures of the measurements are 100 K for **14** (single-crystal, SC), 253 K for **14**, and 353 K for **15**.



	h	k	l	2θ	d
a	0	0	1	6.22	14.242
b	0	1	0	6.58	13.466
c	1	0	0	7.24	12.240
d	1	1	0	7.60	11.661
e	1	1	1	8.88	10.005
f	0	-1	1	8.26	9.574

Figure 8.7. X-ray powder diffractogram of **14**. On top, the inset figure shows an expansion of



the low d value region, which corresponds to the atomic distances. In the table, the major diffraction peaks at high d values are collected. Each peak is assigned to a corresponding h , k , l plane, which is represented in figures a-f below the table. The planes are shown and the arrows indicate the direction of the polymer chains.

8.3.2 Reaction with other solvent molecules.

The exchange of propionitrile in **14** by small molecules other than H₂O has also been explored. Thus, the replacement with acetonitrile or 1-propanol has been found to take place upon immersion of **14** into the corresponding solvent, as judged by the gradual observed decolouration. The XRPD analysis of the products obtained from maintaining **14** in either acetonitrile or 1-propanol for a few days reveal that the guest-exchange occurs without apparent changes in the structure (see Figure 8.8). This observation can be ascribed to the higher structural similarity to propionitrile of the latter two guest-molecules, as compared with water. In addition, acetonitrile and 1-propanol lack the capacity of establishing extended hydrogen bonds that is inherent to water. This feature is considered to be the likely driving force of the structural re-adjustment²³ observed when passing from **14** to **15**. Indeed, structural changes in dynamic porous frameworks caused by the hydrogen bonding properties of incoming guests have been described and reviewed previously.²¹ Especially the case of water has been well studied, showing that its hydrogen-bonding ability is one of the main factors governing the intercalation, and thus the overall structure.²⁴ These interactions may also be at the origin of the higher affinity of **14** for water, as revealed by the fact that the exchange by acetonitrile or 1-propanol molecules in the gas phase could never be effected. On the other hand, more sterically demanding molecules, such as 2-phenylacetonitrile, have not been able to replace propionitrile, at least when using the same conditions as investigated for acetonitrile and 1-propanol. This behaviour provides evidence of the selectivity of **14** towards small linear ligands.²³

8.3 Magnetic behaviour

For the magnetic measurements of **14**, **14**•(propanol) and **14**•(acetonitrile),^b the corresponding samples have been placed in an NMR tube and covered with the minimum amount of mother liquor. The tube is then hermetically closed to avoid the loss of solvent. For measurements above 298 K, a paste (pattex) is used to tightly close the NMR tube. After completion of the measurement, the material is air-dried (resulting in the formation of **15**) and weighed. The resulting amount (moles) of **15** compound involved is thus obtained, and the corresponding mass of the “measured” original material (namely **14**, **14**•(propanol) = [Fe₃(dpyatriz)₂(BF₄)₂(CH₃CH₂OH)₄](BF₄)₄·4(CH₃CH₂OH) or **14**•(acetonitrile) = [Fe₃(dpyatriz)₂(BF₄)₂(CH₃CN)₄](BF₄)₄·4(CH₃CN)) is calculated. This value is then used to determine the corresponding molar magnetic susceptibility.

The fact that the main building block of **14** is a spin-crossover compound (see chapter 6) has supported the expectation that the latter would also exhibit similar properties. Data have been collected under a constant magnetic field of 0.1 T in the 6–370 K temperature range. The results are represented in Figure 8.8 as a $\chi_m T$ vs. T plot, where χ_m is the molar paramagnetic susceptibility per three Fe^{II} ions. At 370 K, the $\chi_m T$ value is 8.60 cm³ K mol⁻¹, in the range expected for three independent HS Fe^{II} ions (9 cm³ K mol⁻¹ for $g = 2$) and already presents a

^b See chapter 2 for details on the experimental procedures and recipes for all compounds presented in this chapter.

positive slope at this temperature. The $\chi_m T$ value continues to decrease quite rapidly upon cooling to reach a near constant value of approximately $3.5 \text{ cm}^3 \text{ K mol}^{-1}$ in the vicinity of 220 K, and only decreases again when the temperature gets close to 10 K, i.e. down to $2.86 \text{ cm}^3 \text{ K mol}^{-1}$ at 6 K. This behaviour suggests the occurrence of a HS to LS spin-crossover process, for only approximately 2/3 of the Fe^{II} centres of the polymer. This is consistent with both iron atoms (Fe2, Figures 8.2 and 8.3) of the dinuclear building block exhibiting the spin transition, as has been previously observed when this moiety was studied as a discrete $[\text{Fe}^{\text{II}}_2]$ complex.¹⁸ In the polymer, the independent Fe1 (Figures 8.2 and 8.3) centre is thus found to remain in the HS state throughout the whole range of temperatures, as expected from the weak ligand field strength of the BF_4^- ligands, causing the wide plateau in the $\chi_m T$ vs. T curve. The decrease in this plot at very low temperatures is most likely due to zero-field splitting of the remaining HS Fe^{II} centres. Interestingly, the thermal spin-crossover observed for **14** is centred at 300 K (ambient temperature).

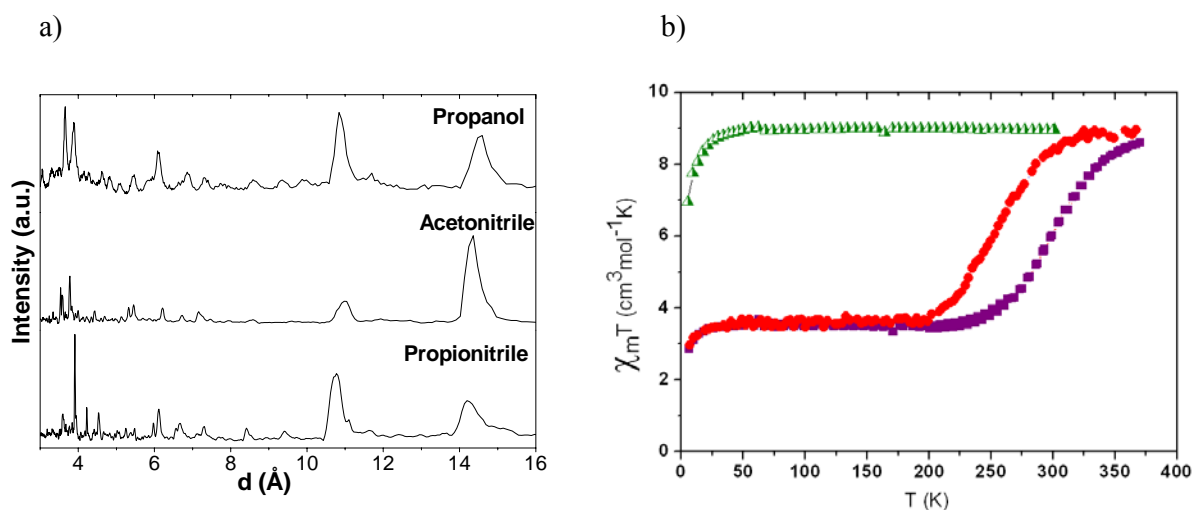


Figure 8.8. a) Comparison of the XRPD patterns for host-guest materials exposed to different atmospheric conditions. Only slight variations are observed when changing the solvent, which indicate that the interplanar distances do not vary significantly. These minor variations are most likely due to the steric similarity of the guest solvent molecules. b) Plots of $\chi_m T$ vs. T per three Fe^{II} ions for **14** (squares), **14** after propionitrile to acetonitrile solvent exchange (circles), and **15** (triangles).

It has been mentioned above that the transformation of **14** into **15** is accompanied by a drastic colour change, from deep purple to pale yellow. This colour change is a clear sign that this chemical process causes a variation of the environment around the Fe2 centres changing the spin state of these ions at room temperature, from LS to HS.²⁴ Indeed, the purple colour is typical for LS octahedral $[\text{FeN}_6]$ coordination compounds, whereas a yellow colour characterises HS octahedral $[\text{FeN}_6]$ complexes. This variation has been studied in detail through variable temperature magnetic susceptibility measurements. A $\chi_m T$ vs. T plot for **15** is depicted in Figure 8.8, showing that the $\chi_m T$ value remains constant, almost throughout the whole range of temperature, at $8.94 \text{ cm}^3 \text{ K mol}^{-1}$, corresponding to three independent HS Fe^{II}

centres, and confirming that the new material has lost the spin–crossover properties of the parent compound. The decrease of $\chi_m T$ observed near 50 K is ascribed to weak antiferromagnetic coupling occurring between the Fe²⁺ HS centres, mediated by the bridging dpyatriz ligands, or to zero-field splitting, as previously documented for this moiety.¹⁸ It is thus clear that the process of transformation of **14** into **15** involves the exchange of labile propionitrile ligands on the Fe²⁺ centres by water molecules, suppressing the spin–crossover properties of these ions. Upon re-absorption of propionitrile, the reverse transformation takes place (see above) and the spin–crossover properties are restored. The system **14/15** constitutes therefore a molecular switch whose magnetic properties are addressable by simply modifying the ambient conditions. The spin–crossover curve of **14** as obtained by re-sorption of propionitrile (from **15**) is less steep than that of a freshly crystallised sample from this solvent (Figure 8.9). This difference is caused by the differences of crystallinity between both samples. Such effects are known to affect the spin-transition behaviour.²⁵

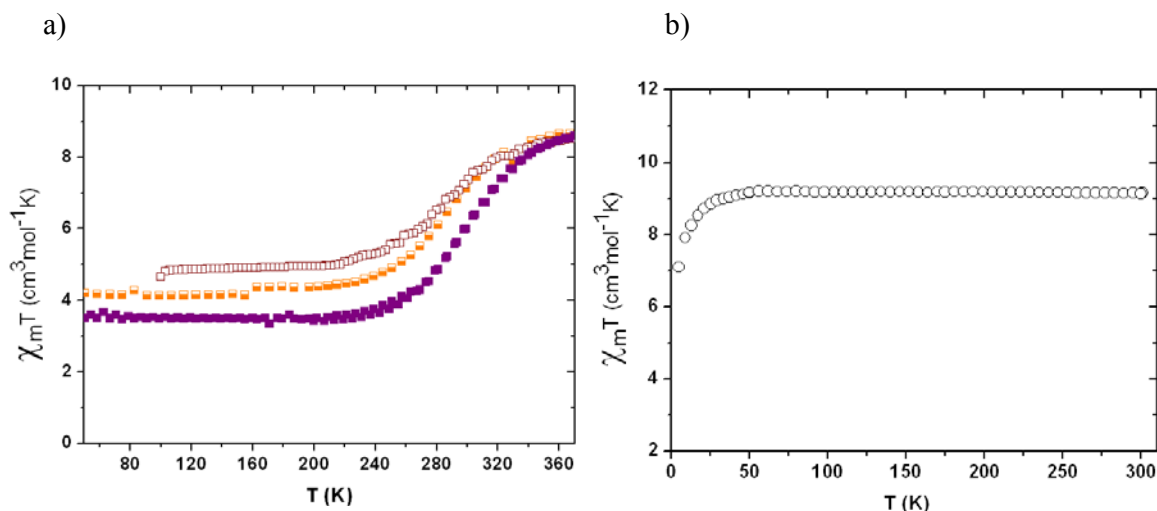


Figure 8.9. a) Plots of $\chi_m T$ vs. T per three Fe^{II} ions for as-synthesised **14** (full squares), **14** (slow reabsorption: semi-full squares) and **14** (reabsorption: empty squares). b) plot of $\chi_m T$ vs. T per three Fe^{II} ions for **14** after exchange of the propionitrile guest molecules with 1-propanol molecules.

The magnetic properties of the material obtained from **14** via substitution of propionitrile by 1-propanol have been examined as well. This substitution leads to almost no change of the structure as deduced from XRPD experiments, but results in total loss of the purple colour. As suggested by this observation, magnetisation measurements have demonstrated that substitution of propionitrile by propanol results in the suppression of the spin–crossover properties in the same manner as occurred with water (see $\chi_m T$ vs. T plot in Figure 8.9). Presumably, the replacement of the nitrile-based ligands of Fe²⁺ by propanol reduces significantly the ligand field around this ion, converting it into a HS species at all temperatures. The case of acetonitrile, by contrast, is different; the $\chi_m T$ vs. T plot (Figure 8.8) shows that the new compound obtained from the exchange with this other solvent maintains the spin–crossover behaviour. The solvent exchange now results in a smaller diminution of the ligand–field, compared to water (i.e. **15**), shifting the transition temperature 20 K towards

lower temperatures (the transition now being centred near 273 K). The steepness of the transition does not change noticeably, in agreement with the observed maintained crystallinity, thus suggesting that the mechanisms of cooperativity throughout the material are preserved.²⁶

8.5 Replacement by non-volatile molecules.

The influence of solvent molecules on spin-transition properties has for long attracted much interest.²⁷⁻²⁹ The narrow range of ligand–field values for which a spin transition is expected makes it very sensitive to any structural modification. In many cases, solvent molecules form part of the second coordination sphere and are not directly coordinated to the metal ion. It is for instance, through their hydrogen bonding network that they induce the electronic or structural modifications responsible for the change in magnetic properties.²⁷⁻²⁹ Although supramolecular chemistry has been greatly developed in the last decades,³⁰ the weak energy of non-covalent interactions makes these systems difficult to predict. Even more, their resulting effect on the spin-transition properties is not always as expected.³¹ Rarer is the case of materials which have accessible metal centres that can be chemically functionalised.¹⁹ These materials offer two advantages over the previous ones; the stronger energy of the coordination bond makes their host-guest chemistry more predictable, and their influence on the electronic properties of the material is more drastic. The nanoporous character and the accessibility of the iron centres of **14**, opens the possibility of studying different molecules (guests) with the intention of modifying both the spin transition and the host-guest chemistry of the material.

With this aim several solvent molecules and anions have been selected and studied. An initial procedure is used with the intention to obtain crystalline materials with which structural information, via X-ray powder diffraction or single crystal X-ray diffraction, can be extracted. In most cases, this procedure has failed for various reasons. In the case of 1-propyltetrazole and 4-amino-1,2,4-triazole ligands, **14** has degraded and ended up forming new materials containing no *dpyatriz* ligand. The slight solubility of **14** in acetonitrile and the greater thermodynamical stability of the resulting compounds could account for such behaviour. For 4-Amino-2,2,6,6-tetramethylpiperidinoxy free radical (amino-tempo) or phenylacetonitrile (benzylcyanide), the small cavities of the compound, as well as the weak coordinating capacity of these ligands make them incapable of replacing the guest molecules in **14**. Small anions, such as SCN^- and Br^- trigger an immediate colour change, assigned to their substitution in the compound. During this process the crystals cracked, leading in the case of Br^- to an amorphous powder and for SCN^- to a more crystalline powder. In both cases, the resulting powder is not homogeneous to the eye (mixture of species) and the corresponding analyses are difficult to interpret. The capacity of the anions to replace not only the BF_4^- counterions, but also the coordinated solvent molecules, would change the overall charge of the system. This difference in charge should cause a structural rearrangement of the solid state structure and a probable mixture of species is to be expected, as has been observed.

These results show that the solvent plays a crucial role in this type of chemistry and a new procedure has been followed. Two new ligands, namely amytriazole (4-pentyl-1,2,4-triazole) and ethyltriazole (4-ethyl-1,2,4-triazole), soluble in toluene (solvent in which **14** is completely insoluble) have been used as guests. **15**, obtained from **14**, is then placed in a toluene solution of the corresponding ligand in excess, and the heterogeneous mixture is stirred for 12 hours, filtered and washed with toluene. These new compounds are named as: **14**·(amyl) and **14**·(ethyl). The IR spectra of the resulting homogeneous white materials show peaks for the *R*-triazole (R = amyl or ethyl) and the *dpyatriz* ligands. The ethyl and amyl chains of the triazole ligands show peaks of C-H vibrations just below 3000 cm⁻¹, while *dpyatriz* shows a characteristic peak of the ring torsion of the triazine ring. It thus appears that the ligand has replaced the coordinated water molecules. Surprisingly, elemental analyses indicate that the triazole/Fe ratio is 2:1. This confirms the replacement of the coordinated water molecules, but also suggests that the coordinated BF₄⁻ anions have also been replaced (see Chapter 2 for analysis). The BF₄⁻ counterions remain present in the crystal lattice to compensate the overall charge of the polymer after the substitution of the neutral triazole-based ligands.

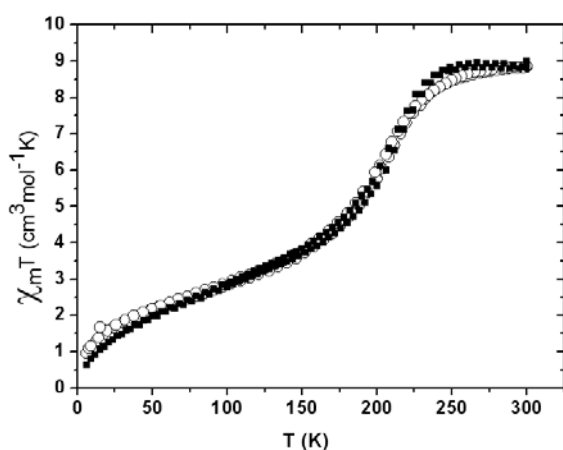


Figure 8.10. $\chi_m T$ vs. T plot of **14**·(amyl) (black squares) and **14**·(ethyl) (white circles).

The magnetic measurements of these materials show a behaviour different from those mentioned above. Figure 8.10 shows the $\chi_m T$ vs. T plot of **14**·(amyl) and **14**·(ethyl), both presenting a similar behaviour. At room temperature, $\chi_m T$ is ca. 8.81 cm³ mol K⁻¹, which is close to the value expected for three independent Fe^{II} ions ($\chi_m T = 9$ cm³ mol K⁻¹, $g = 2$). At temperatures below 250 K, the $\chi_m T$ value gradually decreases, describing a curve with two different parts distinguished by their different slopes. The first part of the curve, which ranges from 300 to ca. 160 K, shows a slope which is similar to those observed in **14** and **14**·(acetonitrile). The $T_{1/2}$ for this first section is 210 K. The second part shows an even more gradual decrease of the $\chi_m T$ value, which at 6 K reaches 0.63 cm³ mol K⁻¹ and 0.96 cm³ mol K⁻¹ for **14**·(amyl) and **14**·(ethyl), respectively. A final decrease is observed at very low temperatures, which is ascribed to zero-field splitting of some remaining HS Fe^{II} centres.

The first decrease in $\chi_m T$ can be assigned to the Fe2 centres, which now have a lower transition temperature than for **14** and **14(acetonitrile)**. The weaker ligand field strength of the triazole ligands stabilises the high-spin state over the low-spin state, and shifts the transition to lower temperatures or even suppresses it, as observed for **14(acetonitrile)**, **15** and **14(propanol)**. The second transition corresponds to the Fe1 centre, which in **14** and **14(acetonitrile)** remained in the HS state over the whole range of temperatures. This seems to confirm that the triazole-based ligands have substituted the BF_4^- anions, as already suggested by the elemental analyses. Although other analyses such as Mössbauer spectroscopy would be necessary to confirm this hypothesis, it seems unlikely that the ligand has not coordinated to the metal ion and therefore has affected the crystal field of Fe1 from the second coordination sphere. The slight overlap of both steps of the transitions could be another indication of the similarity of the coordination spheres, which would only differ in the disposition of the triazole-based ligands (*trans* for Fe1 and *cis* for Fe2).

This second procedure has proved that the solvent dependency of **14** can be stabilised by replacing the corresponding solvent molecules by a non-volatile ligand. Indeed, **14(amyI)** and **14(ethyl)** suffer no chemical modification when left in contact with air and their spin-transition properties thus remain intact. The experimental procedure did not allow obtaining any structural information leading to a clearer explanation. Nevertheless, the elemental analyses, IR and magnetism, point to the replacement of both the coordinated solvent molecules as well as the coordinated anions. The similarity of the spin-transition features of both **14(amyI)** and **14(ethyl)** proves that the alkyl substituent on the triazole ring is not affecting the magnetic properties of the overall materials, as clearly observed in Figure 8.10. All compounds described in this chapter show a similar slope for the first step, which would suggest that the cooperative nature of these systems has an intrapolymeric origin. An improvement of the first procedure can lead to more crystalline substances from which more structural information may be obtained.

8.6 Concluding remarks

The above results demonstrate that **14** constitutes a material whose spin-crossover and chromatic properties can be fine-tuned through a simple mechanism of solvent exchange *via* its nanoporous structure. This exchange leads to reversible and distinct changes to the structure in the case of water, which establishes the link between this material and the so-called *third-generation coordination polymers*.^{21, 23} The latter are defined as flexible nanoporous materials that reversibly accommodate their structure depending on the presence or absence of guest molecules. In the case of **14**, structural variations come about upon solvent exchange, rather than just removal. In this case, it has been demonstrated that the inter-conversion causes drastic effects on the physical properties, and this is due in part to the fact that the process does not only occur for lattice molecules, but also involves ligand exchange. This is due to the nanoporous structure of **14** that enables the access of the external solvent molecules to the magnetically active Fe^{II} centres. The extension of this concept to non-volatile molecules has resulted in the elimination of the solvent dependence of **14**. Moreover, it has been proved that ligands with a stronger binding force can functionalise the

Fe1 centres of the polymeric structure by substituting the BF_4^- anions, and thus modify its electronic properties. The use of different alkyl substituents on the triazole ring has clearly helped to prove that the nature of the cooperativity in this material is intrapolymeric.

In summary, the system described in this chapter has proved that the dinuclear spin-transition compound presented in chapter 6 can be extended to form polymeric species through the free dipyridylamino moieties by applying solvothermal conditions. As for the dinuclear compound, this 1D polymer leaves free coordination sites for solvent molecules to coordinate, which are susceptible to be exchanged, and enables the tuning of the transition temperature. It is thus obvious that making use of the porosity of the system one may influence the magnetic properties of the material. Inversely, the influence of the spin transition on the host-guest chemistry is impossible to determine due to the lack of a crystal structure at high temperatures that would allow the observation of any structural modification of the cavities.

8.7 References

1. Ferlay, S.; Mallah, T.; Ouahes, R.; Veillet, P.; Verdaguer, M., *Nature* **1995**, *378*, 701-703.
2. Kahn, O.; Martinez, C. J., *Science* **1998**, *279*, 44-48.
3. Gütlich, P.; Hauser, A.; Spiering, H., *Angew. Chem. Int. Ed. Engl.* **1994**, *33*, 2024.
4. Real, J. A.; Gaspar, A. B.; Muñoz, M. C., *Dalton Trans.* **2005**, 2062-2079.
5. Niel, V.; Martinez-Agudo, J. M.; Muñoz, M. C.; Gaspar, A. B.; Real, J. A., *Inorg. Chem.* **2001**, *40*, 3838-3839.
6. Uemura, K.; Matsuda, R.; Kitagawa, S., *J. Solid State Chem.* **2005**, *178*, 2420-2429.
7. Yaghi, O. M.; O'Keeffe, M.; Ockwig, N. W.; Chae, H. K.; Eddaoudi, M.; Kim, J., *Nature* **2003**, *423*, 705-714.
8. Zaworotko, M. J., *Angew. Chem. Int. Ed.* **2000**, *39*, 3052-3054.
9. Barthelet, K.; Marrot, J.; Riou, D.; Ferey, G., *Angew. Chem. Int. Ed.* **2002**, *41*, 281-284.
10. Beauvais, L. G.; Long, J. R., *J. Am. Chem. Soc.* **2002**, *124*, 12096-12097.
11. Maspoch, D.; Ruiz-Molina, D.; Veciana, J., *J. Mater. Chem.* **2004**, *14*, 2713-2723.
12. Coronado, E.; Galan-Mascaros, J. R.; Gomez-Garcia, C. J.; Laukhin, V., *Nature* **2000**, *408*, 447-449.
13. Bousseksou, A.; Molnar, G.; Demont, P.; Menegotto, J., *J. Mater. Chem.* **2003**, *13*, 2069-2071.
14. Halder, G. J.; Kepert, C. J.; Moubaraki, B.; Murray, K. S.; Cashion, J. D., *Science* **2002**, *298*, 1762-1765.
15. de Hoog, P.; Gamez, P.; Driessen, W. L.; Reedijk, J., *Tetrahedron Lett.* **2002**, *43*, 6783-6786.
16. de Hoog, P.; Gamez, P.; Roubeau, O.; Lutz, M.; Driessen, W. L.; Spek, A. L.; Reedijk, J., *New J. Chem.* **2003**, *27*, 18-21.
17. Gamez, P.; de Hoog, P.; Roubeau, O.; Lutz, M.; Driessen, W. L.; Spek, A. L.; Reedijk, J., *Chem. Commun.* **2002**, 1488-1489.
18. Quesada, M.; de Hoog, P.; Gamez, P.; Roubeau, O.; Aromì, G.; Donnadièu, B.; Massera, C.; Lutz, M.; Spek, A. L.; Reedijk, J., *Eur. J. Inorg. Chem.* **2006**, 1353-1361.
19. Chui, S. S. Y.; Lo, S. M. F.; Charmant, J. P. H.; Orpen, A. G.; Williams, I. D., *Science* **1999**, *283*, 1148-1150.
20. Roubeau, O.; Haasnoot, J. G.; Codjovi, E.; Varret, F.; Reedijk, J., *Chem. Mater.* **2002**, *14*, 2559-2566.
21. Kitagawa, S.; Uemura, K., *Chem. Soc. Rev.* **2005**, *34*, 109-119.
22. Braga, D.; Curzi, M.; Johansson, A.; Polito, M.; Rubini, K.; Grepioni, F., *Angew. Chem. Int. Ed.* **2006**, *45*, 142-146.
23. Kitagawa, S.; Kitaura, R.; Noro, S., *Angew. Chem. Int. Ed.* **2004**, *43*, 2334-2375.
24. Niel, V.; Thompson, A. L.; Muñoz, M. C.; Galet, A.; Goeta, A. S. E.; Real, J. A., *Angew. Chem. Int. Ed.* **2003**, *42*, 3760-3763.
25. Müller, E. W.; Spiering, H.; Gütlich, P., *Chem. Phys. Lett.* **1982**, *93*, 567-571.
26. Yoneda, K.; Adachi, K.; Hayami, S.; Maeda, Y.; Katada, M.; Fuyuhiko, A.; Kawata, S.; Kaizaki, S., *Chem. Commun.* **2006**, 45-47.
27. Gütlich, P.; Köppen, H.; Steinhäuser, H. G., *Chem. Phys. Lett.* **1980**, *74*, 475.
28. Sorai, M.; Ensling, J.; Hasselbach, K. M.; Gütlich, P., *Chem. Phys.* **1977**, *20*, 197-208.
29. Sugiyarto, K. H.; Craig, D. C.; Rae, A. D.; Goodwin, H. A., *Aust. J. Chem.* **1994**, *47*, 869-890.
30. Lehn, J.-M., *Supramolecular Chemistry: Concepts and Perspectives*. In Wiley-VCH: 1995.

31. Hostettler, M.; Tornroos, K. W.; Chernyshov, D.; Vangdal, B.; Burgi, H. B., *Angew. Chem. Int. Edit.* **2004**, *43*, 4589-4594.